Oth, A., Miyake, H., Bindi, D. (2017): On the relation of earthquake stress drop and ground motion variability. - *Journal of Geophysical Research*, *122*, 7, pp. 5474—5492.

DOI: http://doi.org/10.1002/2017JB014026

AGU PUBLICATIONS

JGR

Journal of Geophysical Research: Solid Earth

RESEARCH ARTICLE
10.1002/2017JB014026

Key Points:
- Stress drops and ground motion between-event residuals are well correlated for crustal earthquakes in Japan
- Higher average stress drop level estimated for Kyushu does not reflect in ground motion between-event residuals
- Combined analysis of stress drops and ground motion between-event residuals holds potential to improve understanding on source variability

Supporting Information:
- Supporting Information S1

Correspondence to:
A. Oth,
adrien.oth@ecgs.lu

Citation:
Oth, A., H. Miyake, and D. Bindi (2017), On the relation of earthquake stress drop and ground motion variability, *J. Geophys. Res. Solid Earth*, *122*, 5474–5492, doi:10.1002/2017JB014026.

Received 25 JAN 2017
Accepted 13 JUL 2017
Accepted article online 15 JUL 2017
Published online 27 JUL 2017

On the relation of earthquake stress drop and ground motion variability

Adrien Oth[1], Hiroe Miyake[2], and Dino Bindi[3]

[1]European Center for Geodynamics and Seismology, Walferdange, Luxembourg, [2]Earthquake Research Institute, University of Tokyo, Tokyo, Japan, [3]Helmholtz Centre Potsdam, GFZ German Research Centre for Geosciences, Potsdam, Germany

Abstract One of the key parameters for earthquake source physics is stress drop since it can be directly linked to the spectral level of ground motion. Stress drop estimates from moment corner frequency analysis have been shown to be extremely variable, and this to a much larger degree than expected from the between-event ground motion variability. This discrepancy raises the question whether classically determined stress drop variability is too large, which would have significant consequences for seismic hazard analysis. We use a large high-quality data set from Japan with well-studied stress drop data to address this issue. Nonparametric and parametric reference ground motion models are derived, and the relation of between-event residuals for Japan Meteorological Agency equivalent seismic intensity and peak ground acceleration with stress drop is analyzed for crustal earthquakes. We find a clear correlation of the between-event residuals with stress drops estimates; however, while the island of Kyushu is characterized by substantially larger stress drops than Honshu, the between-event residuals do not reflect this observation, leading to the appearance of two event families with different stress drop levels yet similar range of between-event residuals. Both the within-family and between-family stress drop variations are larger than expected from the ground motion between-event variability. A systematic common analysis of these parameters holds the potential to provide important constraints on the relative robustness of different groups of data in the different parameter spaces and to improve our understanding on how much of the observed source parameter variability is likely to be true source physics variability.

1. Introduction

The appropriate understanding and modeling of earthquake source physics plays a key role in the prediction of ground shaking that has to be expected from future earthquakes. As a rule, empirically calibrated ground motion prediction equations (GMPEs) are used to this end. These GMPEs relate a set of response variables such as peak ground acceleration (PGA) or velocity (PGV), response spectra, or other seismic intensity measures to the main predictor variables magnitude and distance. They furthermore often involve additional predictor variables for taking into account site conditions and faulting style (a comprehensive review of the principle features of GMPEs is provided by *Douglas* [2003]). Besides the tuning of the originally rather simple functional forms of GMPEs with additional model terms to incorporate a vast range of effects into their prediction capabilities (e.g., short-distance saturation, magnitude-dependent attenuation, and nonlinear site amplification—see, for instance, the GMPE models derived in the context of the PEER NGA-West2 project [*Bozorgnia et al*., 2014, and references therein]), the aleatory variability of ground motions, generally expressed in terms of the standard deviation (sigma), has gained significant attention. This is because it has been recognized that it is actually the variability of the ground motions around their median rather than the level of the median itself that exerts the largest influence on probabilistic seismic hazard estimates, in particular at long return periods [e.g., *Bommer and Abrahamson*, 2006].

The question then arises whether it is possible, in a legitimate way, to decrease the sigma of GMPEs for the purpose of site-specific hazard assessment. *Anderson and Brune* [1999] put into question the so-called ergodic assumption, and *Atkinson* [2006] showed that the single-site standard deviation is smaller than the overall standard deviation from a regression over a broad network of stations. *Al Atik et al*. [2010] discussed how the variability of GMPEs can be split into different components, and the key to a potential reduction of sigma lies in the detection of any systematic trends and the understanding of their origins, such that these could be "transferred" into the epistemic uncertainty treatment. Further studies have investigated this separation of residuals with different data sets [e.g., *Rodriguez-Marek et al*., 2011; *Chen and Faccioli*, 2013; *Luzi et al*., 2014], with particular emphasis on the discussion on single-station sigma. Another fundamental aspect in this

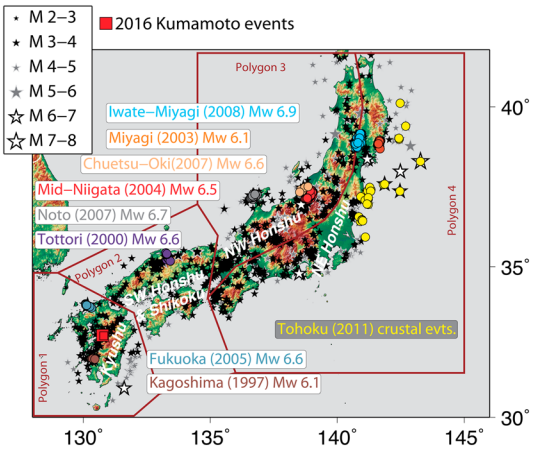

Figure 1. Epicenters of earthquakes used in this study. Extracted individual earthquake sequences are color coded following the main shock name. Note that the 2011 Tohoku main shock (M_W 9.0) is not included in the analysis and only crustal aftershocks of this event are considered here. The regions as discussed in the text are provided (Kyushu, SW Honshu, NW Honshu, and NE Honshu) and defined through the polygons shown. The 2016 Kumamoto events are marked by red squares.

discussion, however, lies in the quantification and potential removal of systematic source-related variability components. Besides the effect of rupture directivity, which is persistently observed even for small earthquakes [*Boatwright*, 2007; *Kane et al*., 2013] and taken into account with various strategies in GMPEs [e.g., *Bozorgnia et al*., 2014; *Kurzon et al*., 2014], the effect of stress drop ($\Delta\tau$) on ground motion variability has gained increased attention [*Baltay et al*., 2013; *Cotton et al*., 2013].

Following *McGuire and Hanks* [1980] and *Hanks and McGuire* [1981], we can relate PGA and $\Delta\tau$ assuming that acceleration time histories have the phase characteristics of stationary, band-limited white noise. This implies that the $\Delta\tau$ variability can in principle be determined from the between-event variability of GMPE models for PGA [*Cotton et al*., 2013]. $\Delta\tau$ in turn is traditionally estimated from seismic moment (M_0)-corner frequency (f_C) analysis of earthquake spectra, typically under the assumption that the ω^{-2} model [*Aki*, 1967; *Brune*, 1970, 1971] holds. There are various approaches to estimate these parameters, such as the empirical Green's functions (EGF) approach [e.g., *Mayeda et al*., 2007; *Abercrombie*, 2013] or the generalized inversion technique to derive earthquake source spectra [e.g., *Drouet et al*., 2008; *Oth et al*., 2011b]. Regardless of which approach is used, the obtained $\Delta\tau$ values show large variability and are in particular very sensitive to errors in f_C, since $\Delta\tau \propto f_C^{3}$. *Cotton et al*. [2013] noted that the $\Delta\tau$ variability estimated from such source studies is by far too large relative to the expectation arising from the between-event ground motion variability estimated from GMPE models. This discrepancy raises the question how much of the $\Delta\tau$ variability from classical M_0-f_C studies is actually representative of true source variability. The answer to this question may have significant implications for ground motion prediction in seismic hazard assessment, since $\Delta\tau$ values from such studies are often used as input for ground motion simulations, for instance, with the stochastic technique [*Boore*, 2003].

Cotton et al. [2013] raised the issue by looking at the standard deviation values of the GMPE between-event variability and usually large $\Delta\tau$ samples from various source studies in the literature, and some physical explanations have been invoked to explain the observed discrepancy. *Causse and Song* [2015] concluded that in contrast to the usually assumed independence of stress drop and rupture velocity, these quantities would most likely have to be anticorrelated to explain the observed between-event ground motion variability. *Archuleta and Ji* [2016] use a two-corner moment rate function to explain the scaling of PGA and PGV. They argue that since the stress parameter controlling peak ground motions (controlled by the peak time of their source time function) is not the same as M_0-f_C determined stress drop (controlled by the rupture duration), their variability also does not necessarily need to be the same. However, the details of the correlation between between-event residuals and $\Delta\tau$ (beyond their respective standard deviations) have not yet been widely explored.

$\Delta\tau$ has been observed to show spatially coherent variations, for instance, in California [*Shearer et al*., 2006] or in Japan [*Oth*, 2013]. While these variations are generally not simple to explain, *Oth* [2013] noted that these lateral variations in Japan correlate with lateral heat flow variations. Two further interesting observations were also made in the latter study: (1) On the local scale of individual earthquake sequences, the $\Delta\tau$ variability is significantly smaller than on the scale of the entire Japanese archipelago, and (2) the island of Kyushu (Figure 1) seems to clearly set apart [see *Oth*, 2013, Figure 2] in terms of stress drop, with on average 1 order of magnitude higher $\Delta\tau$ values for crustal earthquakes as compared to the rest of Japan (Figure 2).

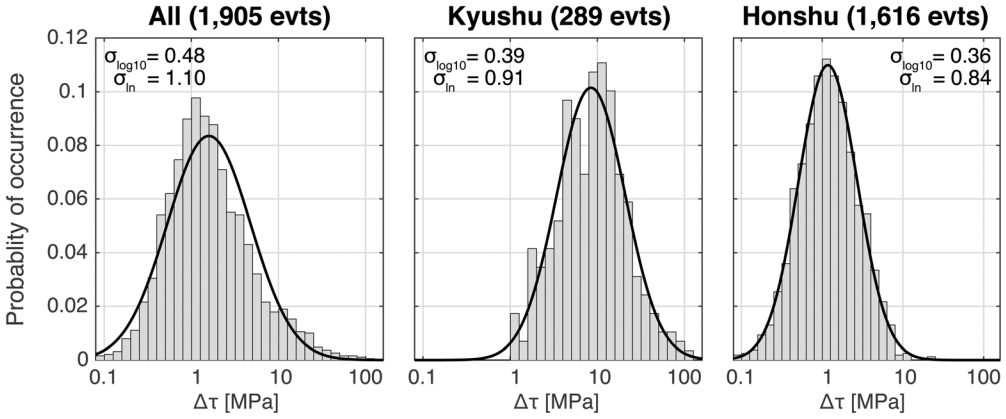

Figure 2. $\Delta\tau$ histograms for (left) all crustal earthquakes combined, (middle) events in Kyushu, and (right) events in Honshu (SW, NW, and NE Honshu, Figure 2, right) derived from spectral inversion and M_0-f_C analysis [*Oth*, 2013]. The black line depicts the best fitting lognormal distribution function, and the standard deviations in log 10 and natural logarithm bases are indicated in the upper corner of the plots.

In this article, we build on these results from *Oth* [2013] to improve our understanding of the generally observed discrepancies between $\Delta\tau$ and ground motion variability. Specifically, we explore whether the $\Delta\tau$ variations in Japan reflect in the between-event variability of ground motion parameters in a pattern consistent with the above mentioned observations. We compare not only the standard deviations of $\Delta\tau$ and ground motion between-event term distributions but investigate the relationship between these parameters in detail. In addition, since the origin of the elevated $\Delta\tau$ values in Kyushu is difficult to explain from a tectonic perspective, this study provides additional constraints on how much of these high-$\Delta\tau$ results in Kyushu represent true source variability or are potentially due to other reasons.

To this end, we analyze the variability of equivalent Japan Meteorological Agency (JMA) instrumental intensity ($I_{JMA,\ equiv.}$) [*Shabestari and Yamazaki*, 2001] and PGA for crustal earthquakes applying a nonparametric as well as a parametric mixed-effects regression approach to the data. With the obtained models, we characterize the between-event variability for 1905 events throughout Japan (M_w range 2.7–7.2) and compare the distribution of these between-event terms with the $\Delta\tau$ distribution obtained by *Oth* [2013], with a particular emphasis on the difference in regional behavior between Kyushu and Honshu. $\Delta\tau$ and between-event ground motion variability for the recent 2016 Kumamoto earthquake (M_w 7.1) and its largest foreshock (M_w 6.1) [*Asano and Iwata*, 2016; *Kubo et al*., 2016] are also briefly discussed in the context of these models. We observe that while the $\Delta\tau$ values in Kyushu are significantly larger than in Honshu, the between-event residuals cover the same range of values in these two regions. We discuss the potential reasons for the generation of these two data families and compare the within-family stress drop variability with the corresponding between-event ground motion variability.

2. Data

The data set under investigation is composed of recordings from the K-NET and KiK-net accelerometric networks in Japan, whose instruments have an almost flat response from DC to 30 Hz [*Okada et al*., 2004; *Aoi et al*., 2011]. It covers the time period May 1996 to October 2011 and includes the same events as used in the spectral source study presented by *Oth* [2013]. In particular, the $\Delta\tau$ estimates from the latter study are used. These $\Delta\tau$ values were obtained by calculating source spectra using a generalized inversion technique followed by spectral fitting to determine M_0 and f_C. For details on this processing, we refer the reader to *Oth et al*. [2011a, 2011b] and *Oth* [2013]. Seismic moments for the largest events with JMA magnitude $M_{JMA} \geq 5$ were taken from the National Research Institute for Earth Science and Disaster Resilience centroid moment tensor solutions catalog (http://www.fnet.bosai.go.jp), and it was ensured that seismic moments for small and large events are compatible by choosing appropriate spectral fitting parameters [see *Oth*, 2013]. The two events during the 2016 Kumamoto earthquake sequence, i.e., the M_w 6.1 foreshock and the M_w 7.1 main shock, were not used for the regression analysis outlined below but for residual analysis using the models derived without them (see section 4) and are therefore not counted here.

Table 1. Finite-Source Rupture Models Chosen for the Calculation of Rupture Distance for Events in the Data Set Where Such Models Were Available in the Literature

Event Name	Event ID	M_w	Reference
Kagoshima (1997)			
First event[a]	9703261731	6.1	*Horikawa* [2001]
Second event[a]	9705131438	6.0	*Horikawa* [2001]
Tottori (2000)[a]	0010061330	6.6	*Iwata et al.* [2000]
Geiyo (2001)[a]	0103241528	6.8	*Sekiguchi and Iwata* [2001]
Miyagi (2003)[a]	0307260713	6.1	*Miuara et al.* [2004]
Mid-Niigata (2004)			
Main shock[a]	0410231756	6.5	*Asano and Iwata* [2009]
First major aftershock	0410231803	6.0	*Hikima and Koketsu* [2005]
Second major aftershock	0410231812	5.7	*Hikima and Koketsu* [2005]
Third major aftershock	0410231834	6.3	*Hikima and Koketsu* [2005]
Fourth major aftershock	0410271040	5.8	*Hikima and Koketsu* [2005]
Fukuoka (2005)[a]	0503201053	6.6	*Asano and Iwata* [2006]
Noto (2007)[a]	0703250942	6.7	*Asano and Iwata* [2011]
Chuetsu-Oki (2007)[a]	0707161013	6.6	*Cirella et al.* [2008]
Iwate-Miyagi (2008)[a]	0806140843	6.9	*Cultrera et al.* [2013]
Suruga Bay (2009)	0908110507	6.2	*Aoi et al.* [2010]
Tohoku (2011) foreshock[a]	1103091145	7.2	*Hayes* [2011]
Nagano-Niigata (2011)	1103120359	6.2	*Hata et al.* [2012]
Kumamoto (2016)			
Largest foreshock	1604142126	6.1	*Kobayashi et al.* [2016]
Main shock	1604160125	7.1	*Kobayashi et al.* [2016]

[a]Models taken from the SRCMOD finite-fault rupture database [*Mai and Thingbaijam*, 2014].

The database includes 118,102 records from 1905 crustal events (depth $\leq$ 30 km) with M_w values ranging between 2.7 and 7.2 (Figure 1), of which 38,226 are recorded at borehole sensors of the KiK-net array and 79,876 are surface recordings (K-NET and KiK-net). These records were obtained at 1411 sites, including 581 KiK-net sites with a borehole sensor. Borehole sensors are treated as separate stations in the processing, leading to a formal total of 1992 stations. Only data with hypocentral distances lower than 250 km were considered, with the requirement that each event was recorded by at least three stations and each station recorded at least three events. While for the source spectra calculation only weak and not too strong motion data (PGA $<$ 0.2 g) at hypocentral distances of 5 km or larger were considered in order to minimize nonlinear soil amplification and near-field effects [*Oth et al.*, 2011b; *Oth*, 2013], we did not impose such a constraint for the ground motion analysis in this study, yet the number of such records is quite limited.

Events from nine major earthquake sequences since 1997 are also grouped together (Figure 1) in order to study the sequence-to-sequence variability of ground motions between these. Events were associated with a given sequence if they occurred in a time window of 6 months following the main shock and within a lateral range of one estimated fault length and one estimated fault width in depth [*Oth*, 2013]. For the Tohoku aftershocks at crustal depths, we only used events that were located within the estimated fault plane (Figure 1). We are aware that these events are plate interface events and not in-land crustal earthquakes, yet still include them in the analysis for the sake of completeness.

As distance metric, we use hypocentral distance R_{hypo} for small and moderate events, thus assuming a point source in first approximation. For the largest earthquakes with near-source recordings, however, the finite-fault size needs to be taken into account. We therefore collected finite-fault source models in the literature for the largest events in the data set for which such models were available to calculate the closest distance to the rupture, R_{rup} (Table 1), in particular using the SRCMOD finite-source rupture database [*Mai and Thingbaijam*, 2014]. This way we were able to characterize with R_{rup} all data from events with $M_w \geq 6$, only missing four offshore events (M_w 5.9–6.5) for which such finite-fault models were not available and where hypocentral distance is an acceptable distance metric even for earthquakes of that size. For small and moderate earthquakes where the point source approximation is acceptable in view of the source-to-site distances and considered frequency range, R_{hypo} is considered as an equivalent estimate of R_{rup}.

Table 2. JMA Seismic Intensity Scale and Relation With Instrumentally Obtained Values (I_{JMA})[a]

JMA Intensity Scale	I_{JMA} Range	Approximate MMI Range of Given JMA Intensity Level
0	$I_{JMA} < 0.5$	I
1	$0.5 \le I_{JMA} < 1.5$	I–II
2	$1.5 \le I_{JMA} < 2.5$	II–IV
3	$2.5 \le I_{JMA} < 3.5$	IV–VI
4	$3.5 \le I_{JMA} < 4.5$	VI–VII
5−	$4.5 \le I_{JMA} < 5.0$	VII–VIII
5+	$5.0 \le I_{JMA} < 5.5$	VIII–IX
6−	$5.5 \le I_{JMA} < 6.0$	IX–X
6+	$6.0 \le I_{JMA} < 6.5$	X–XI
7	$6.5 \le I_{JMA}$	X–XII

[a]Approximately corresponding MMI intensity levels [*Kodera et al*., 2016] are provided in the last column.

For the purpose of this study, we calculate and analyze the ground motion parameters PGA (geometric mean of horizontal components) as well as the so-called JMA equivalent seismic intensity. Based on the work of *McGuire and Hanks* [1980] and *Hanks and McGuire* [1981], the following relationship can be derived between PGA and $\Delta\tau$ [*Baltay et al*., 2013; *Cotton et al*., 2013]:

$$\mathrm{PGA} = \frac{2R_{\theta\phi}(2\pi)^2\Delta\tau}{106\rho R}\sqrt{\frac{f_{\max}}{f_C}}\sqrt{2\ln\left(\frac{2f_{\max}}{f_C}\right)}, \quad (1)$$

where $\Delta\tau$ is the stress drop, $R_{\theta\phi}$ is the radiation pattern, ρ is the density, R represents the distance measure between source and site, $f_{\max}$ is the observational upper frequency limit of the recordings, and f_C is the corner frequency of the earthquake under consideration. Based on equation (1), earthquake stress drop variability should translate directly and predictably into PGA variability.

Seismic intensity (e.g., modified Mercalli or JMA seismic intensity [*Musson and Cecić*, 2012]) is an interesting parameter from an operational point of view since it provides easily understandable information about the distribution of damage or, more generally, earthquake effects. Instrumental intensity measures, i.e., inferred from ground motion observations rather than macroseismic questionnaires or field surveys, can in particular very rapidly provide such information, for instance, in the framework of ShakeMap calculations [e.g., *Wald et al*., 1999], and are as a rule calibrated to be compatible with some macroseismic intensity scale.

In Japan, JMA seismic intensity is the most widely used scale, covering 10 degrees from 0 to 7 (Table 2). Estimates based on instrumental data, from either so-called intensity meters or classical strong-motion records, are usually referred to as JMA instrumental intensity (I_{JMA}). I_{JMA} is estimated using three-component accelerometric records (see *Shabestari and Yamazaki* [2001] for a detailed description). In a first step, the three acceleration time histories are transformed into Fourier domain and a band-pass filter with corner frequencies 0.5 and 10 Hz is applied to the data. This band-pass filter is designed in order to emphasize the ground shaking around 0.5–1 Hz related to wooden frame house damage in Japan during large earthquakes, while the strong falloff above 10 Hz ensures that frequencies above this threshold are practically completely ignored [*Sokolov and Furumura*, 2008]. After filtering, the records are transformed back to time domain by inverse Fourier transform and the vectorial sum of the three components is calculated. Finally, a reference acceleration value a_0 is calculated such that the total duration where this threshold is exceeded is equal to 0.3 s. I_{JMA} is finally obtained using the equation

$$I_{JMA} = 2\ \log a_0 + 0.94. \quad (2)$$

Besides its easily interpretable relation to earthquake effects, I_{JMA} is also an interesting parameter for our study in view of the fact that in contrast to PGA, it also includes information on the (band-pass-filtered) acceleration pulse duration and is a widely used ground motion parameter in Japan. In operational routine at JMA, this calculation procedure is performed for every 10 s of the continuous data streams, and then the maximum value for a given earthquake is chosen. In this work, we apply the above calculation procedure to the complete earthquake records, which leads to practically identical results. In order to identify this calculation difference, however, we refer to the values calculated in this article as equivalent JMA instrumental intensity, $I_{JMA,\ equiv.}$. Figure 3 shows the data distribution in terms of magnitude and distance, magnitude and depth,

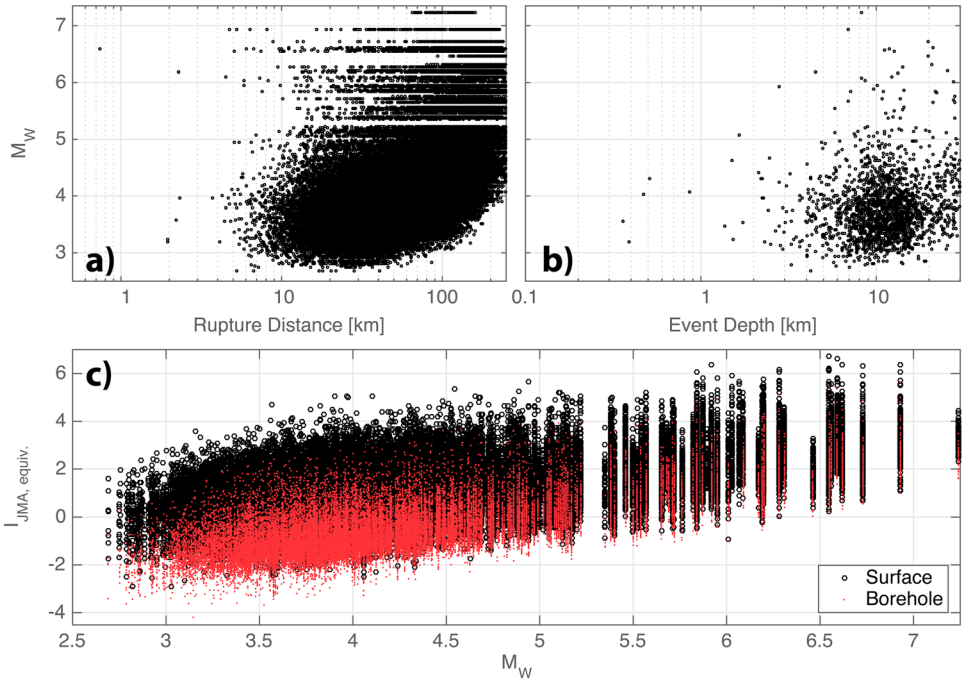

Figure 3. Data set distribution in terms of (a) M_w versus rupture/hypocentral distance (see text), (b) M_w versus earthquake depth, and (c) $I_{JMA,\ equiv.}$ versus M_w. In the latter plot; black circles indicate surface data, while red dots show borehole records. Distances from 5 to 250 km are well covered by data, and the majority of events took place at depths between 5 and 20 km.

and magnitude and $I_{JMA,\ equiv.}$. Data are well distributed over the entire magnitude range and for distances larger than about 5 km. Some data points at shorter distances are available for both small and large events, but they are rather sparse. In terms of event depths, most events range between 5 and 20 km. To no surprise, borehole $I_{JMA,\ equiv.}$ values are significantly smaller than those at the corresponding surface sensors, showing the strong influence of site response [*Oth et al*., 2011a, 2011b] on ground shaking intensity.

3. Regression and Analysis Methods

We apply two different regression approaches to the data in order to determine robust median ground motion models describing the magnitude and distance dependence and then isolate the between-event residuals in relation to these models. The first approach is a nonparametric regression technique. Nonparametric regression is widely applied for the inversion of earthquake ground motion Fourier amplitude spectra to separate frequency-dependent source, path, and site response characteristics [*Oth et al*., 2011b, and references therein]. The prime advantage of this type of technique lies in the fact that no a priori assumptions are made on the functional form of the different components of the model. This technique is therefore particularly well suited for data sets with excellent distance and magnitude coverage. Here we use essentially the same method as for spectral inversion, using, however, ground motion parameters ($I_{JMA,\ equiv.}$ and PGA) as input variables. A similar approach has been used by *Bindi et al*. [2011] for deriving intensity prediction equations for central Asia.

The second approach is the more traditional parametric regression framework commonly used in GMPE development. Here a parametric model with a well-defined function form is set up, and the parameters of this model are determined through parametric regression such as the two-stage method of *Joyner and Boore* [1981] or random effects approaches [*Abrahamson and Youngs*, 1992; *Chen and Tsai*, 2002]. *Stafford* [2014] showed that mixed-effects concepts can be used to go far beyond the usually considered linear additive random effects in the quest for ergodic assumption removal, allowing, for instance, taking into account region-to-region variations in attenuation parameters. In this work, however, we only focus on linear additive random effects related to the traditional definition of the between-event variability [*Al Atik et al*., 2010; *Cotton et al*., 2013].

3.1. Nonparametric Ground Motion Model

Similar to *Bindi et al*. [2011], we model the ground motion input variable under consideration with the following relation:

$$Y_k\left(M_W, R_{\text{rup}}\right) = S_i + w_l A_l + (1 - w_l)A_{l+1} + G_j, \tag{3}$$

where Y_k is given by the kth observation of the ground motion measure to be considered, i.e., $I_{\text{JMA, equiv.}}$ or $\log_{10}$ (PGA), with $k = 1{:}\ldots{:}N_{\text{data}}$, N_{data} being the total number of ground motion observations from N_{eq} earthquakes at N_{site} stations. R_{rup} is the distance (rupture/hypocentral as described above), S_i stands for the source term of earthquake i, with $i = 1{:}\ldots{:}N_{\text{eq}}$, while A_l represents the attenuation term for the bin l with distance value r_l, where $l = 1{:}\ldots{:}\text{N}_{\text{bins}}$. For each event-station pair, the lth distance bin is chosen such that $r_l \leq R_{\text{rup}} < r_{l+1}$, and the weights are given by $w_l = (R_{\text{rup}} - r_l)/(r_{l+1} - r_l)$ such that the attenuation curve is linearized between the distances r_l and r_{l+1}. Finally, G_j is a site response term for station j (not included in the analysis of *Bindi et al*. [2011]). The above system of equations is solved using a one-step least squares inversion approach [*Oth et al*., 2011b]. Three constraints are applied in order to remove trade-offs between source, attenuation, and site terms and to stabilize the inversion for distance bins not well covered by data: (1) the attenuation function is constrained to take a zero value at 10 km distance, (2) attenuation is constrained to be a smooth function with distance (implemented through a second-derivative constraint [*Castro et al*., 1990]), and (3) the average site response of all borehole sensors is supposed to be equal to unity (i.e., borehole sites on average amplification free). We derive these nonparametric models for each of the regions of interest individually (i.e., Kyushu, SW Honshu, NW Honshu, and NE Honshu) as well as for all regions combined.

The distance bins used here are chosen to be 2 km wide, covering the distance range 0–250 km. Several weight values for implementing the strength of the smoothing constraint were tested in order to find the best balance between suppressing strong short-distance variations in A while avoiding biases in the overall trends. The stability of the solution was tested using a bootstrap approach [*Oth et al*., 2011b]. To this end, we calculated 100 bootstrap replications of the original data set and investigate their mean and standard deviation. On average, the bootstrap-estimated errors range around 3–5% for the source terms and 6–10% for the site terms, depending on the number of recordings. For the attenuation terms, the estimated error remains well below 1% for distances larger than 15 km and increases up to around 40% as distance decreases (not considering the 10 km distance bin since this was constrained be equal to 0). This simply reflects the fact that there are fewer records at short distances. Note, however, that these error estimates for the attenuation bins depend on the strength of the smoothing constraint.

The source terms S_i obtained with this approach represent in fact the ground motion resulting from event i at the reference distance of 10 km for the site reference condition (i.e., average borehole ground motion). In order to quantify the between-event variability of these source terms, we fit an appropriate magnitude-dependent model to the S_i values and calculate the between-event residuals as the deviation for each S_i from the predicted value at the given magnitude of event i. We found that a quadratic model represented an appropriate fit (see section 4), and the between-event residuals can be expressed as

$$\delta B_e = S_i - \left[b_0 + b_1 M_{W,i} + b_2 M_{W,i}^2\right], \tag{4}$$

where $b_{0,1,2}$ represent the coefficients of the quadratic fit obtained by nonlinear least squares. The site-to-site variability of the terms G_j can be investigated by grouping the stations with respect to their National Earthquake Hazards Reduction program (NEHRP) site classes, depending on the estimates available for the shear wave velocity of the upper 30 m, v_{S30} [*Building Seismic Safety Council*, 2003]. For KiK-net stations, these estimates were retrieved directly from the shear wave velocity profiles. For K-NET stations, profiles do not extend beyond a depth of 20 m, and in this case, we use the v_{S30} values determined by *Boore et al*. [2011] considering regional correlations of v_{S30} with velocities averaged over smaller depth ranges, using K-NET and KiK-net data in their analysis.

The ranges of site term values G_j for surface stations grouped according to their various NEHRP site classes are shown in terms of box and whisker plots in Figure 4 for $I_{\text{JMA, equiv.}}$ and PGA. As expected, amplification effects increase significantly from site class A (hard rock) to site classes D/E (stiff/soft soil). The site response contributes substantially to the overall observed seismic intensity, with amplification effects increasing the

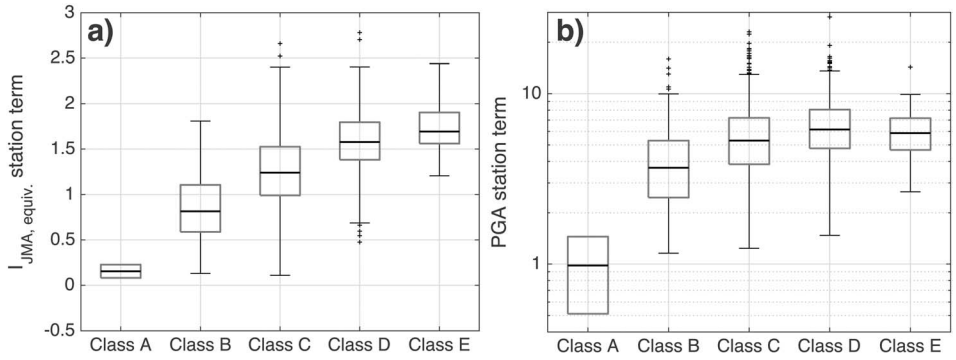

Figure 4. Box and whisker plots for station terms G_j (see also equation (3)) obtained for (a) $I_{JMA,\ equiv.}$ and (b) PGA. Sites are classified according to NEHRP site classes using their v_{S30} values (A, $v_{S30} > 1500$ m/s; B, $760 < v_{S30} \leq 1500$ m/s; C, $360 < v_{S30} \leq 760$ m/s; D, $180 < v_{S30} \leq 360$ m/s; E, $v_{S30} \leq 180$ m/s). In this figure only surface stations are considered. Median values are represented as black lines, the gray boxes denote the quartiles, and the whiskers correspond to a coverage of 99.3% of the data points. Data outside this range are considered as outliers and plotted individually as crosses.

intensity values relative to hard rock by up to 2, in some cases even 2.5 to 3 intensity units. The same pattern can be observed for PGA, where estimated amplification values for site class E are slightly smaller than for site class D, probably reflecting some nonlinear site response effects. Note, however, that there are comparatively few sites classified as site class E, with only 75 such sites in the data set as compared with 481 sites classified as D. Since this article focuses on the between-event variability of the source component, we do not further discuss the details on the site response variability, such as the spatial distribution and the within-class variability.

3.2. Parametric Mixed-Effects Regression Approach

As a benchmark for cross-checking the nonparametric results, we derive a parametric ground motion model for the data set by applying a nonlinear mixed-effects regression approach (NLMER) [e.g., *Bates et al.*, 2014], as also described by *Kotha et al.* [2016]. In terms of functional form for the fixed effects, we use the typical basic components [e.g., *Boore et al.*, 2014] and define the following parametric model, from which we will, however, eliminate the terms with parameters c_2 and c_3 as outlined below:

$$Y = e_0 + F_D(R_{\text{rup}}, M_w) + F_M(M_w) + \delta B_{\text{seq}} + \delta B_e + \delta B_{s-\text{class}} + \delta B_s + \varepsilon, \tag{5}$$

$$F_D(R_{\text{rup}}, M_w) = [c_1 + c_2(M_w - M_{\text{ref}})] \log\left(\frac{\sqrt{R_{\text{rup}}^2 + h^2}}{R_{\text{ref}}}\right) + c_3\left(\sqrt{R_{\text{rup}}^2 + h^2} - R_{\text{ref}}\right), \tag{6}$$

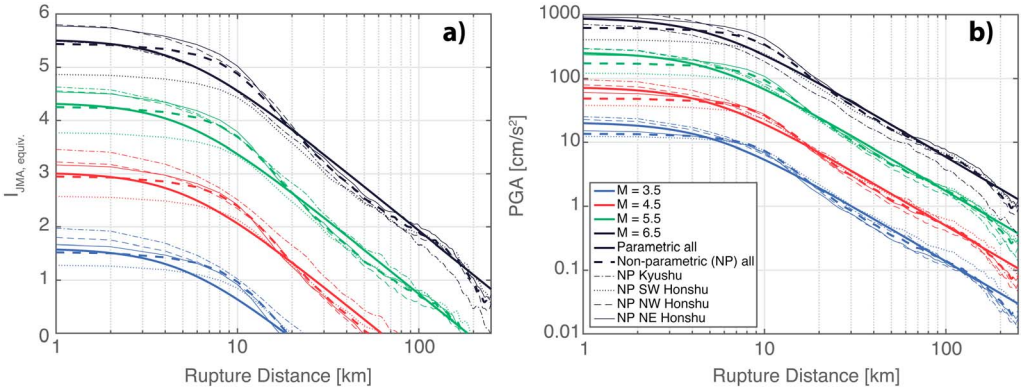

Figure 5. Median ground motion models (nonparametric and parametric) for average borehole site conditions, (a) for $I_{JMA,\ equiv.}$ and (b) for PGA. Different line styles indicate different models as indicated in the legend, while color indicates different magnitude values.

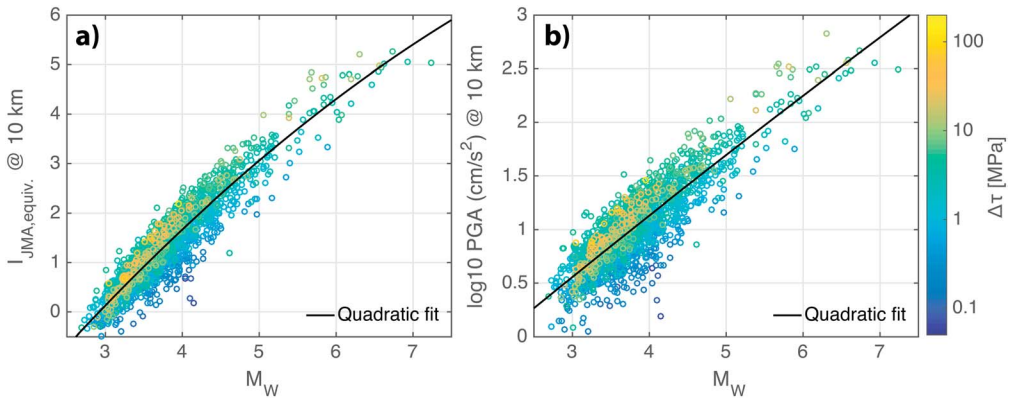

Figure 6. Magnitude dependence of the nonparametric source terms S_i (see also equation (3)), (a) for $I_{JMA,\ equiv.}$ and (b) for PGA. Data points are color coded following their $\Delta\tau$ values, and the black line indicates the fitted quadratic magnitude dependence following equation (2).

$$F_M(M_w) = \begin{cases} b_1(M_w - M_h) + b_2(M_w - M_h)^2 \text{ for } M_w < M_h, \\ b_3(M_w - M_h) \text{ for } M_w \geq M_h \end{cases} \quad with\ M_h = 6.5, \tag{7}$$

where Y represents the observed ground motion variable as in equation (3) and F_D and F_M are the distance and magnitude components, respectively. Parameters e_0, c_1, c_2, c_3, b_1, b_2, b_3, and h are the fixed-effects components of the model, while δB_{seq}, δB_e, $\delta B_{s\text{-class}}$, and δB_s represent the random effects components on parameter e_0 describing the between-sequence, between-event, between-site-class, and between-station variability, respectively. While in the nonparametric analysis these variability components can be analyzed from the residual distribution of equation (4) relative to the respective reference models (as is also still common practice for parametric models), the mixed-effects framework in the parametric case has the advantage that these random effects can be added in a natural, statistically more correct, way.

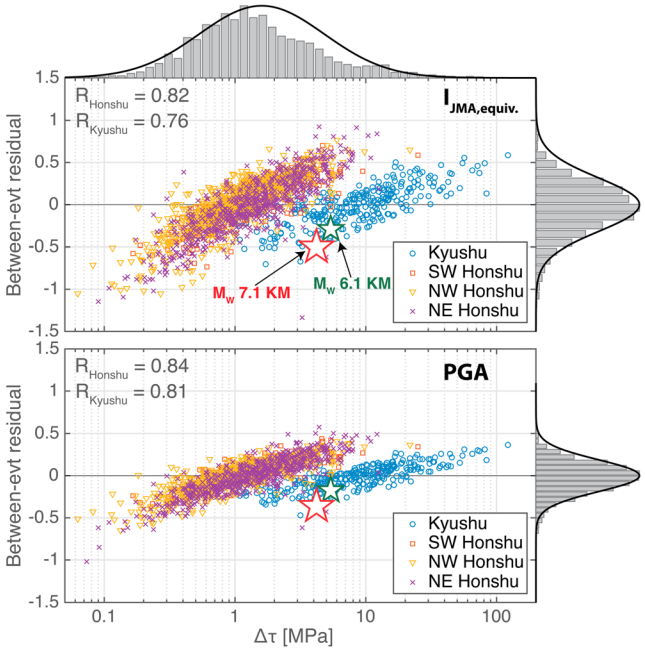

Figure 7. Between-event residuals δB_e resulting from the nonparametric regression approach versus $\Delta\tau$ for (top) $I_{JMA,\ equiv.}$ and (bottom) PGA. Data points are color coded following their region of origin (Figure 1), and their histograms and the estimated distribution functions (black lines) are shown on the right for δB_e and top for $\Delta\tau$, respectively. Note the two data families centered around $\delta B_e = 0$ for Honshu and Kyushu. The two 2016 Kumamoto events are indicated as red and green stars with white face color. The correlation coefficients for two families are given in the upper left corner of each plot (R_{Honshu} and R_{Kyushu}).

During several regression tests, we noted that the regression coefficients tended to be highly unstable if the pseudodepth h was treated as a free regression parameter. For this reason, we tested several fixed values as well as a magnitude-dependent exponential term, and finally fixed its value to $h = 5$ km. Since h controls the ground motion saturation of the model at short distances, the instability issue most likely arises due to the small number of short distance data points available. In addition, the c_2 term tends to trade off with the

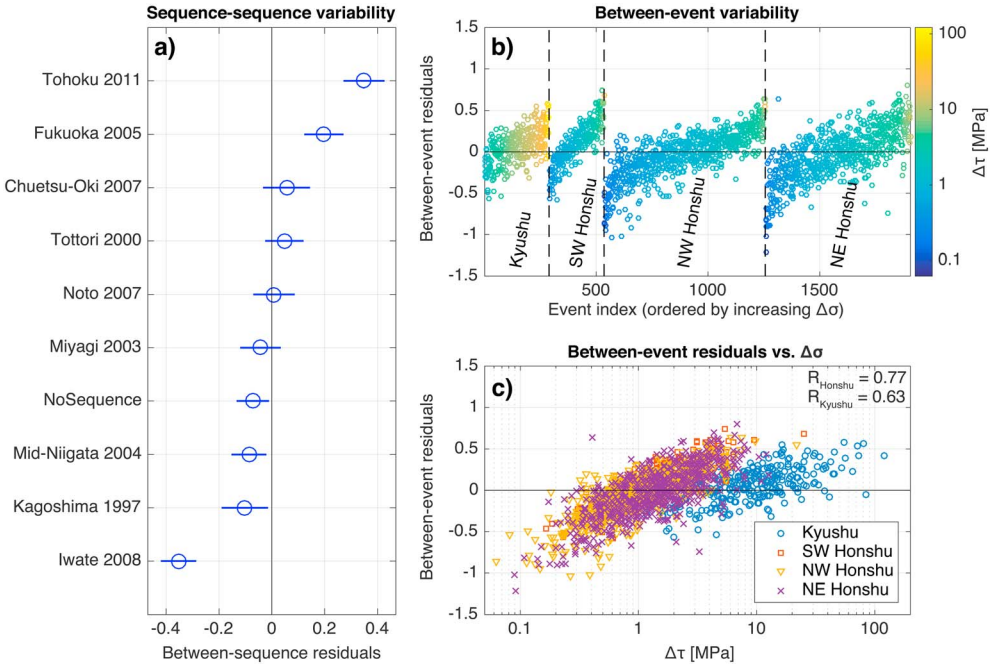

Figure 8. Results from the parametric mixed-effects regression procedure on the $I_{JMA,\ equiv.}$ data. (a) Between-sequence residuals δB_{seq} (see also equation (5)) for the individual earthquake sequences extracted from the data set (Figure 1). (b) Between-event residuals δB_e color coded and ordered with increasing stress drop in each of the four analyzed regions. (c) δB_e versus $\Delta\tau$ color coded by region; see also Figure 7 for the corresponding nonparametric case. The correlation coefficients for two families are given in the upper right corner (R_{Honshu} and R_{Kyushu}).

pseudodepth, because both terms influence the prediction of the level of Y at zero distance. In order to allow for a robust retrieval of both these parameters, a very rich data set at short distance would be required, which is unfortunately not the case in this study. For this reason, we decided to drop the magnitude-dependent c_2 term in the geometrical spreading part of the model.

Finally, c_3 tended to be either statistically indistinguishable from 0 or turned out to be positive, which is why we dropped this anelastic attenuation term. The hinge magnitude M_h was kept as a parameter in the model, even though set to a value of 6.5; there will only be few events affected by this change in scaling, and this effect was not considered in the magnitude scaling function used for the nonparametric source terms.

3.3. Important Notes on These Simple Models

With the ground motion models presented above, we do not aim at developing a GMPE for use in hazard calculations but at defining robust reference models to better understand the between-event variability of ground motion relative to the observed scatter in $\Delta\tau$ estimates. We therefore deliberately keep these models simple and do not attempt to parameterize complex effects that only affect small subsets of the large database, such as nonlinear site response. Directivity effects can generally be expected to average out in the framework of between-event residual calculations. For the parametric model, the short-distance saturation is difficult to properly constrain as discussed above. Although this is an issue of prime importance for ground motion prediction at short distances for hazard assessment, the accuracy of these predictions does not play a significant role for the purpose of this article, and only few recordings are affected by this issue. In the nonparametric model, short-distance saturation will be accounted for more naturally since this model is much more data driven. However, at distances shorter than 5 km, the smoothing constraint will be the driving factor due to the lack of data, and the distance dependence in this range should be considered as speculative.

The overall robustness of the models can be assessed by plotting the residuals versus magnitude and distance (Figures S1–S4 in the supporting information of this article). The nonparametric residuals do not show any trend with distance and magnitude, except some degree of overprediction for the few data points at very short distances, as can be expected. No substantial bias is visible for the parametric case either; however, the residuals indicate some degree of overprediction at very large distances ($>$ ~180–200 km), slight

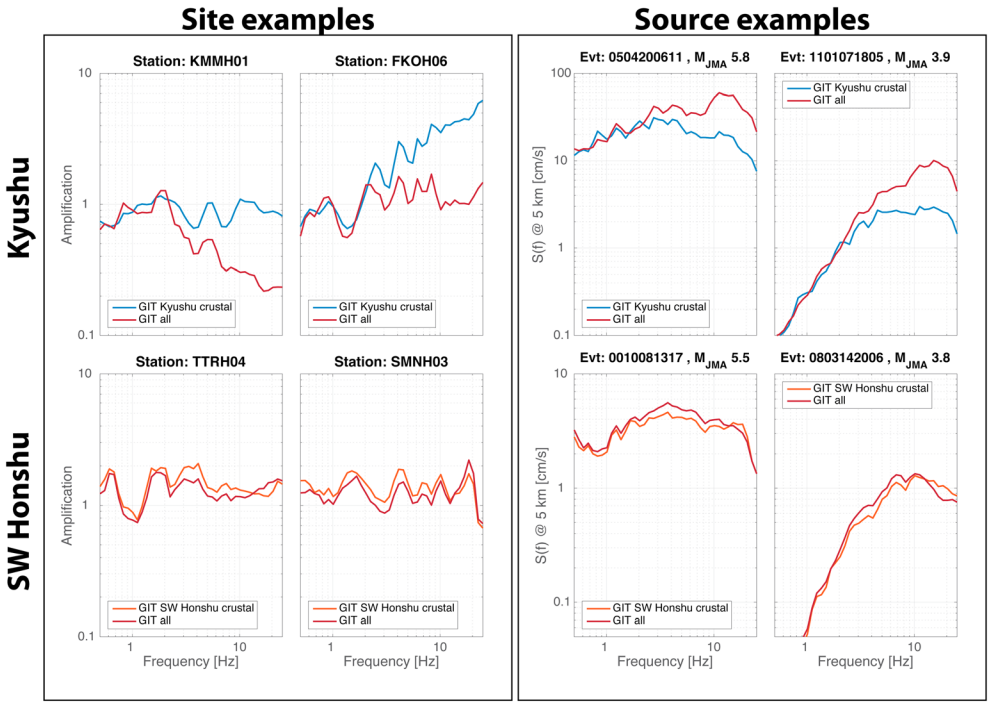

Figure 9. Examples of (left) site response functions and (right) source spectra resulting from nonparametric generalized inversion technique analysis (GIT). (top row) Comparison of GIT results for two sites and two sources located in Kyushu and well covered by data for the cases that (1) we use only data from crustal earthquakes in Kyushu and the regional average of borehole stations as reference and (2) the results of the Japan-wide GIT as described in *Oth* [2013]. (bottom row) Same for two sites and sources in SW Honshu. While for SW Honshu the results are nearly identical, the Kyushu results show an apparent trade-off between source and site functions.

underprediction in the distance range 5–15 km, and similar to the nonparametric case, some overprediction at very short distance. These differences between nonparametric and parametric residuals are in good agreement with the differences in average ground motion prediction by these models shown in Figure 5. Naturally, the nonparametric model is able to capture attenuation variations with distance that cannot be modeled with the prescribed functional form of the parametric case. Overall, these residual distributions show that the models derived provide an appropriate representation of the average trends within the data set for the purpose of this study.

4. Results

4.1. Median Ground Motion Models and Magnitude Scaling

The nonparametric and parametric median ground motion models for average borehole conditions (in the nonparametric case, this was the site reference condition; in the parametric case, a specific site class was defined for borehole sensors) are shown in Figure 5. These models provide indications that there are some regional differences in ground motion attenuation with distance, which seems slightly more pronounced for $I_{JMA,\ equiv.}$ than for PGA. Predicted $I_{JMA,\ equiv.}$ values for SW Honshu are consistently smaller than in other regions, in particular, at moderate and large magnitudes. The SW Honshu function also shows a trend toward stronger saturation at short distance, even though this trend should be interpreted with caution since it is not well constrained by data. For small to moderate magnitudes, predicted $I_{JMA,\ equiv.}$ values in Kyushu tend to be larger than for the other regions, whereas this effect gradually vanishes with increasing magnitude. This tendency is not visible for PGA, which may imply that the ground motions in Honshu are characterized by somewhat shorter acceleration pulses than in Kyushu, with similar PGAs but smaller a_0 values as defined in equation (2) (Figure S5 in the supporting information of this article). This observation could be indicative of slightly higher rupture velocities for small earthquakes in Honshu. The nonparametric model shows that attenuation with distance is somewhat more complex than can be modeled by a simple parametric geometrical spreading term (c_1, equations (5)–(7)), with a larger slope at intermediate distance (~10–50 km) and a

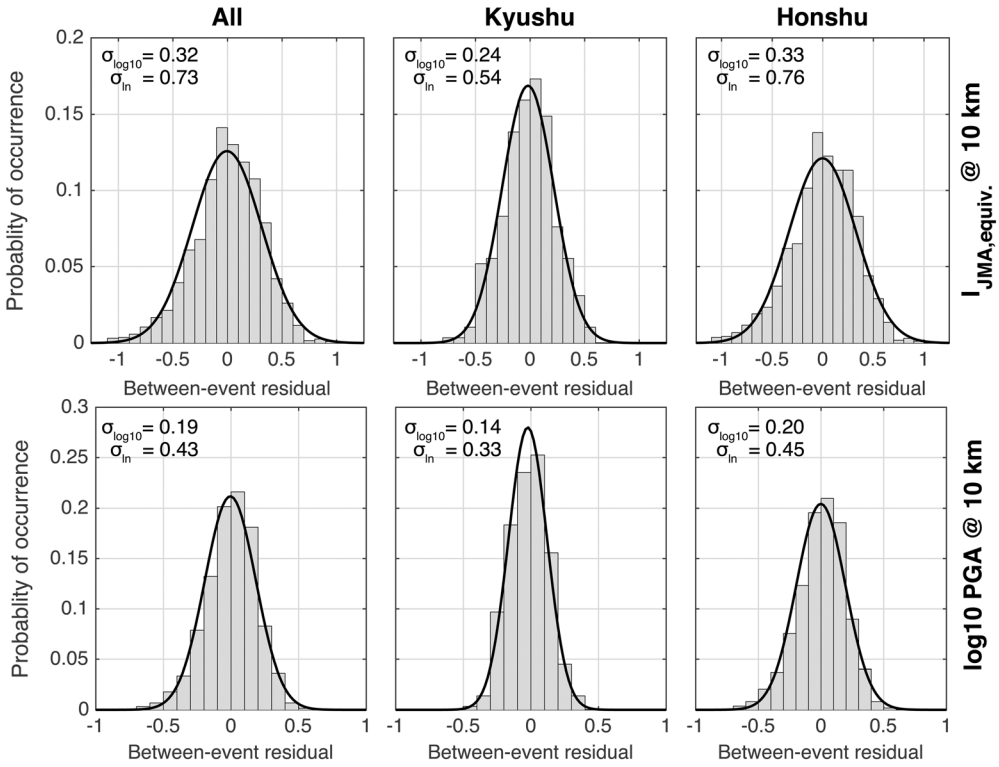

Figure 10. δB_e histograms for (top row) $I_{JMA,\ equiv.}$ and (bottom row) PGA for (left column) all regions together, (middle column) Kyushu, and (right column) the three regions in Honshu. The black lines indicate the fitted normal distribution function in each case, and standard deviations are given in log10 and natural logarithm bases for each case.

subsequent decrease in slope (~50–150 km). This effect cannot be appropriately captured with an additional anelastic term (c_3, equations (5)–(7)), which may explain the encountered issues during the regression calculations. Despite these differences, the nonparametric and parametric models are overall consistent in their predictions in distance and magnitude ranges well covered by data.

The magnitude scaling is well characterized by a quadratic function for the nonparametric case (Figure 6). Based on these nonparametric results, we decided to introduce a hinge term [e.g., *Boore et al*., 2011] in the parametric description since the largest events in the database provide evidence for saturation. However, this conclusion is essentially based on the two largest events only, and up to M_w 6.5, the scaling is essentially quadratic, with the linear term dominating (especially for PGA). The resulting source scaling from the parametric regression is consistent with the nonparametric result. While this difference in scaling at highest magnitude will cause a difference in the δB_e values for these specific events between the nonparametric and parametric approaches, this difference is not of major significance for the discussion in this article, which focuses on the general relationship between δB_e and $\Delta\tau$ measurements.

In Figure 6, the source terms S_i are color coded following their $\Delta\tau$ as derived by *Oth* [2013]. For a given magnitude, there is a clear trend for increasing S_i values with increasing $\Delta\tau$, both for $I_{JMA,\ equiv.}$ and PGA. However, from about $\Delta\tau$ = 10 MPa upward, it seems that there is no significant increase anymore. Almost all these very high $\Delta\tau$ events are located on the island of Kyushu, which is the motivation to investigate the regional dependence between δB_e and $\Delta\tau$.

4.2. Between-Event Variability and Stress Drop Dependence

Figure 7 depicts the between-event residuals δB_e from the nonparametric regression analysis (equation (4)), i.e., the deviation of the source terms S_i from the average quadratic magnitude scaling (Figure 6), plotted versus event stress drop $\Delta\tau$. Events are color coded following their location in the four regions Kyushu, SW Honshu, NW Honshu, and NE Honshu (Figure 1). For both $I_{JMA,\ equiv.}$ and PGA, there is a clear regional correlation between δB_e and $\Delta\tau$. The dependence is stronger yet with more scatter in the case of $I_{JMA,\ equiv.}$ as

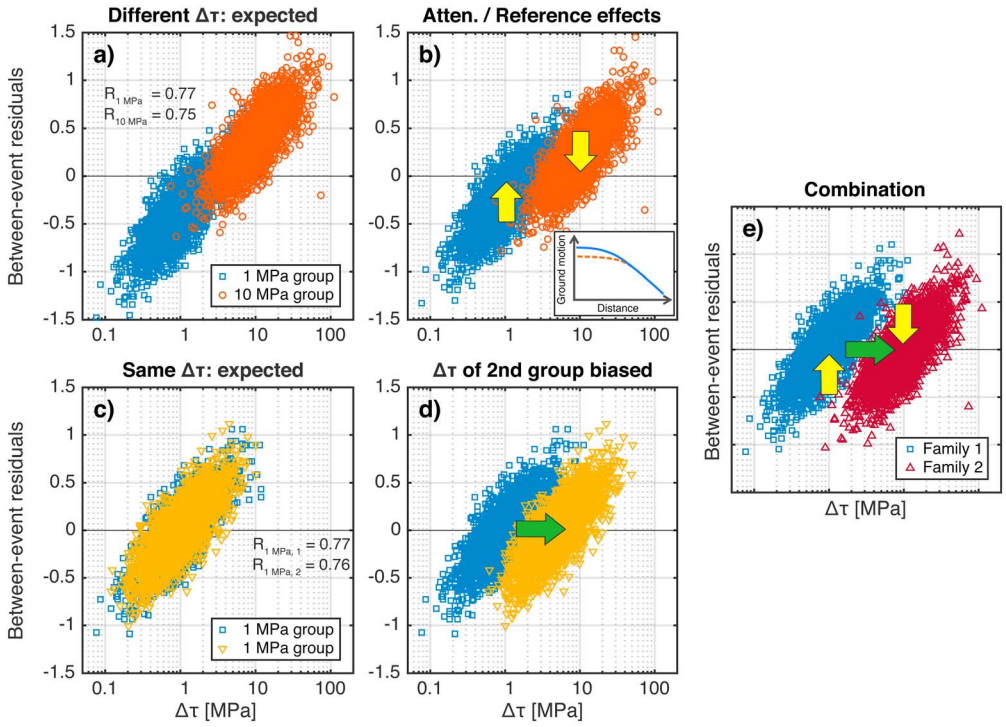

Figure 11. Schematic figure to illustrate the conceptual discussion based on synthetic between-event residual data (see text for details) to explain effects observed in Figures 7 and 8c. (a) Expected distribution of δB_e data in the case of two data groups with lognormal $\Delta\tau$ distributions with mean values of 1 and 10 MPa, respectively. (b) Introduction of δB_e bias due to near-source attenuation differences (inset) or reference condition effects leads to vertical shift between groups and generation of two families in plot. (c) Expected distribution of δB_e data in the case of two data groups drawn from the same lognormal $\Delta\tau$ distribution with mean value of 1 MPa. (d) Introduction of $\Delta\tau$ bias leads to horizontal shift between groups and generation of two families in plot. (e) Schematic illustration of both effects combined. The correlation coefficients for each family are given in Figures 11a and 11c, respectively.

compared with PGA. The trend is consistent between the three regions covering the island of Honshu, with $\delta B_e = 0$ for $\Delta\tau \sim 1$ MPa. This result implies that the median ground motion model shown in Figure 5 represents the ground motion prediction for a ~ 1 MPa (i.e., the median $\Delta\tau$ in Honshu, Figure 2) earthquake and borehole site conditions.

From a theoretical point of view, one would now expect in Figure 7 to find the high stress drop data points from Kyushu as a continuation of this trend observed for the lower stress drop data families for Honshu (see section 5). However, this is not the case, and the data from Kyushu form a separate family in this plot, covering a smaller range in δB_e values centered around 0, with $\delta B_e = 0$ for $\Delta\tau \sim 10$ MPa, which roughly represents the median $\Delta\tau$ in Kyushu. While the $\Delta\tau$ distribution shown in Figures 2 and 7 is not well approximated by a lognormal distribution, the δB_e are normally distributed (which is of course expected for the regression procedures). However, if taken separately, $\Delta\tau$ values in Honshu and Kyushu are roughly log normally distributed (Figure 2), and their combination leads to a bimodal distribution dominated by Honshu, since there are significantly more events from Honshu contributing to the data set.

The parametric results confirm the trends observed above for the nonparametric study (Figure 8, showing the parametric results for the case of $I_{JMA,\ equiv.}$, and Figure S6 in the supporting information for PGA). In addition to the between-event variability, we here also show the between-sequence variability of $I_{JMA,\ equiv.}$. The largest between-sequence increase in predicted $I_{JMA,\ equiv.}$ is observed for events belonging to the 2011 Tohoku sequence (excluding the M_w 9.0 main shock) and the 2005 Fukuoka sequence, which are both characterized by high $\Delta\tau$. In contrast, the strongest between-sequence decrease is related to the 2008 Iwate sequence, which is consistently characterized by some of the lowest $\Delta\tau$ values in the data set. Although the general trends of the between-sequence variability are consistent with the $\Delta\tau$ observations, the 1997 Kagoshima sequence in southern Kyushu is an exception to this rule. It is characterized by the second largest

between-sequence ground motion decrease (Figure 8a) but depicts larger $\Delta\tau$ values than all sequences in Honshu.

4.3. The 2016 Kumamoto Earthquake

The 2016 destructive Kumamoto earthquake (M_w 7.1) and its large foreshock (M_w 6.1) [*Asano and Iwata*, 2016; *Kubo et al*., 2016] are interesting events in the context of this study, since they occurred in western Kyushu and provide two important additional data points for the study of between-event residuals. In order to check their consistency with the results obtained with the described regression analysis, we calculated their stress drop following the processing steps outlined by *Oth et al*. [2011b] and *Oth* [2013] and the between-event residuals relative to the above nonparametric model. The result of this analysis is shown in Figure 7. The Kumamoto main shock has $\Delta\tau$ and δB_e values of 4.5 MPa and -0.5 $I_{\mathrm{JMA,\ equiv.}}$ units, while the foreshock has $\Delta\tau$ and δB_e values of 5.2 MPa and -0.3 $I_{\mathrm{JMA,\ equiv.}}$ units. The results are within the bottom third of the Kyushu data family, implying that for their estimated stress drop values, these events showed comparatively low $I_{\mathrm{JMA,\ equiv.}}$ and PGA values. However, the main shock's magnitude lies at the upper bound of our considered magnitude range, and therefore the results for this event should be viewed with some caution.

5. Discussion and Conclusions

While all the data from the three subsets in Honshu show a consistent behavior, the structure of the two families (Honshu versus Kyushu) observed in the between-event residuals discussed above is intriguing because it would in principle imply that the predicted ground motion, be it $I_{\mathrm{JMA,\ equiv.}}$ or PGA, is the same for a 1 MPa earthquake in Honshu and a 10 MPa earthquake in Kyushu. In view of the fact that (1) the modeled ground motion attenuation with distance does not show significant regional variations and (2) the stress drop calculations have been carried out taking into account potential attenuation variations (found not to be strong) from source spectra determined relative to a Japan-wide site reference condition [*Oth*, 2013], this result seems difficult to explain. The most evident possible explanation would lie in the fact that all stress drop values of crustal earthquakes in Kyushu derived from generalized spectral inversion might be biased high. Note that even though the Kyushu data form this separate family in Figures 7 and 8c, there is still a clear correlation relation between $\Delta\tau$ and δB_e within the Kyushu family.

The source spectra and hence stress drops in Japan have been determined relative to a common reference condition for the entire country, i.e., relative to assumption that on average, the borehole recordings are amplification free over the entire frequency band of analysis (0.5–25 Hz). However, if two regions are only weakly connected by data (i.e., by source-site travel paths), it could happen that the trade-off between source spectra and site response terms may not be adequately solved, depending on possible peculiarities in the events or stations connecting the regions. While all regions in Honshu are well-connected by data, the connection between SW Honshu and Kyushu is overall rather weak. Furthermore, while Kyushu has only one neighboring region within the data set, each region in Honshu is interconnected with two neighboring regions. In the generalized inversion by *Oth* [2013], both crustal and subcrustal events were included, and Kyushu is connected to SW Honshu through more subcrustal than crustal events recorded in both regions.

To assess the potential impact of the weak connection between Kyushu and SW Honshu, we ran separate nonparametric spectral inversions for crustal events in Kyushu and SW Honshu and compare them to the source spectra and site response functions determined through Japan-wide separation [*Oth*, 2013]. In Figure 9, we show the examples of two site response functions and two source spectra well covered by data in Kyushu and SW Honshu. While in SW Honshu the results of the Japan-wide and region-specific inversions are nearly identical, this is not the case in Kyushu at high frequencies. Indeed, Figure 9 highlights a trade-off in source spectra and site response terms between the two inversions, most likely resulting from the inversion prioritizing the fitting of the common subcrustal event spectra and consequently adapting the site spectra and crustal event spectra accordingly. This outcome shows that there must be some differences in ground motions levels in Kyushu relative to Honshu (since otherwise the separation relative to the common reference would not give different results than relative to individual inversion), possibly due to an unaccounted difference in subcrustal paths attenuation between Honshu and Kyushu since the effect tends to get stronger with increasing frequency. This result provides indications that the $\Delta\tau$ values for crustal earthquakes in Kyushu are most likely biased high relative to Honshu, which would explain the generation of the two

families. In light of these observations, the absolute $\Delta\tau$ values in Kyushu should be regarded with extreme caution, including the 2016 Kumamoto events as shown in Figure 7. They are consistent with the Kyushu family since they have been calculated using the site response functions from the Japan-wide source-site separation.

Figure 9 also shows that such weakly interconnected regions may pose unexpected problems for generalized spectral inversions (as well as ground motion regression approaches, since the approaches are very similar). If source spectral biases between different subgroups of the data are present, this effect may contribute significantly to the overall $\Delta\tau$ standard deviation. It is interesting to note in this context that *Cotton et al*. [2013] list the $\Delta\tau$ standard deviations for several large-scale studies based on spectral separation techniques to determine event source spectra, and that all these studies show similar $\Delta\tau$ standard deviations. This issue deserves an in-depth investigation and will be the subject of a dedicated study, since its detailed discussion goes far beyond the scope of this work.

Following the above results, looking at the $\Delta\tau$ and δB_e variability within each observed data family is a more robust approach than simply looking at the overall standard deviations. *Cotton et al*. [2013] showed that under the assumption that equation (1) and the classical omega-square model hold, one would expect that in terms of natural logarithm, the standard deviations of $\Delta\tau$ and PGA δB_e should be related as $\sigma_{\ln(\Delta\tau)} = 6/5\ \sigma_{\ln(PGA)}$. Therefore, looking at the distributions in Figure 10, we would expect a $\sigma_{\ln(\Delta\tau)}$ value of about 0.54 and 0.40 natural-log units for Honshu and Kyushu, respectively. The $\Delta\tau$ distributions for Honshu and Kyushu show, however, standard deviations of 0.84 and 0.91 natural-log units, respectively. While the latter values are significantly smaller than the standard deviation obtained for all of the data set (not surprisingly, as this involves mixing groups of data with largely different medians), they are still larger than expected from the δB_e distribution by a factor of 1.5 to 2.3, respectively. This implies that the data clouds in terms of $\Delta\tau$-δB_e data pairs seen in Figure 7 would be expected to show a steeper relationship. It is also interesting to note that while the standard deviation of the $\Delta\tau$ distribution in Kyushu is not smaller than in Honshu (Figure 2), the standard deviation of the δB_e is substantially smaller in Kyushu (Figure 10).

Finally, in order to provide a conceptual discussion on the observed effects and the potential pitfalls in comparing the $\Delta\tau$ and δB_e variability, we generate synthetic data based on equation (1). For a suite of M_w values ranging from 2 to 7 with steps of 0.2 units, we draw 100 samples at each magnitude from three lognormal stress drop distributions to generate three groups of data points: (1) a group with mean 1 MPa and standard deviation of 0.3 log-$\Delta\tau$ units; (2) a group with mean 10 MPa and standard deviation of 0.3 log-$\Delta\tau$ units; and (3) another group with mean 1 MPa and standard deviation of 0.3 log-$\Delta\tau$ units. We use these $\Delta\tau$ samples in equation (1) to calculate the expected PGA at a fixed distance of 10 km (same as the reference distance in nonparametric regression—thus the log of these PGA values essentially correspond to the source terms S_i in equations (3) and (4)). In equation (1), we set $f_{\max}$ to 30 Hz, $R_{\theta\phi}$ to 0.55, and ρ to 2.9 kg/m^3, and corner frequencies are calculated using a shear wave velocity v_S of 3 km/s [*Oth*, 2013]. On these estimated PGA values, we add normally distributed random noise in log space with standard deviation of 0.2 $\log_{10}$ units. Finally, we fit an average quadratic magnitude scaling term using nonlinear least squares to these synthetic data and use equation (4) to calculate the between-event residuals δB_e.

Figure 11a shows the expected behavior of δB_e for the two groups with median $\Delta\tau$ of 1 and 10 MPa, respectively. If these data are combined in a common regression analysis, we would expect that the δB_e show one continuous trend in terms of $\Delta\tau$ rather than two separate families centered around 0 as we obtained in Figure 7. Note that as mentioned previously, the trend of the synthetic data for each family is steeper than observed, i.e., the observed correlation is weaker than expected.

If the two data groups under discussion arise from the same $\Delta\tau$ distribution with a median of 1 MPa, the self-evident expectation is that they cover the same $\Delta\tau$-δB_e range (Figure 11c). In that case, the only possibility to generate the two-family structure observed in Figure 7 is also evident, as discussed above: a bias in $\Delta\tau$ measurements for one of the two groups relative to the other (Figure 11d). Shown in the figure is the schematic example of a bias of a factor 5, i.e., the $\Delta\tau$ values for the yellow data group are supposed biased high by a factor 5. Such a bias is easy to get, since $\Delta\tau$ depends on f_C^3, and thus we only need a bias of a factor 1.7 in f_C, in view of issues as discussed above for generalized spectra inversions as well the potential pitfalls of empirical Green's functions (EGF) approaches (which are prone to bias, for instance, due to the usage of

inappropriate EGF earthquakes or depending on whether a given earthquake is used as main shock or EGF event, issues discussed by *Abercrombie* [2013, 2015]). Note that since stress drops are calculated using the corner frequencies from the source spectra, they require unbiased estimates of the source spectra over a wide bandwidth in order to be unbiased as well.

Another well-known issue that may affect source spectral estimates at high frequencies and thus also stress drop estimates is the typically observed high-frequency diminution of earthquake amplitude spectra, often expressed through the κ [*Anderson and Hough*, 1984] or f_{max} [*Hanks*, 1982] terms (see also *Ktenidou et al*. [2014], for a review on this effect and its engineering significance). We have accounted for this effect in the calculation of the source spectra and stress drop estimates, and for a detailed discussion on this matter, we refer the reader to *Oth et al*. [2011b]. Note that also the vast majority of $\Delta\tau$ has been derived using borehole data only, which are far less sensitive to this high-frequency diminution effect. While we cannot entirely rule out that unaccounted κ decays may still contribute to some extend to a bias in $\Delta\tau$ values, this cannot be the primary reason of the observed shift between the two families in terms of $\Delta\tau$. Indeed, the bias introduced by an unaccounted κ decay would be expected to show a strongly magnitude-dependent characteristic, with a more pronounced effect of f_C underestimation for decreasing event magnitude [*Anderson*, 1986]. Hence, we would expect that the estimated f_C values would stop or at least slow down increasing at some point with decreasing magnitude. Such an effect has not been observed by *Oth et al*. [2011b] or *Oth* [2013].

On the other hand, even if the $\Delta\tau$ values can be assumed to be unbiased, this still does not mean that nothing can go wrong. One could still generate the observed two families by essentially shifting one or both groups of data along the vertical, i.e., through a mechanism causing bias in the between-event residuals (Figure 11b). This could, for instance, arise from unresolved near-source attenuation effects that are different in the two groups, as schematically indicated in the inset. If short distances are not well sampled, which is often the case, the differences in near-source attenuation properties as well as stress drop between the two groups of events may be underestimated or even unrecognizable in the between-event residuals. This would result in a rather narrow distribution of δB_e, while $\Delta\tau$ values would cover a wide range of values, consistent with the observations of *Cotton et al*. [2013], and even within a given data family, such an effect could explain why the correlation of δB_e and $\Delta\tau$ is not as strong as expected.

Another possible mechanism that could cause such bias in between-event residuals lies, similar to the generalized spectral inversion case, in the reference conditions relative to which the ground motion model is determined. Especially data sets used for GMPE regression analysis often contain data from disconnected or weakly connected regions (an example is the NGA-West2 database, containing data, for instance, from California, Taiwan, Japan, and Turkey). It could, for instance, happen that for some of these regions, all or part of the ground motion data are significantly higher or lower than in other regions given their common site classes. The regression algorithms can accommodate such data sets by simply adjusting groups of between-event residuals in trade-off with the between-site residuals, if not appropriately taken into account, for instance, in the mixed-effects framework as suggested by *Stafford* [2014]. For the Japan case, we show the site terms from the nonparametric regressions relative to the reference condition (see equation (3)) in Figure S7 in the supporting information. While difficult to see when borehole and surface stations are combined, a look at the borehole site terms alone reveals that for $I_{JMA,\ equiv.}$, a small such effect is visible between the average site terms of Kyushu and SW Honshu, which are only weakly interconnected, yet by itself not large enough to explain the two families seen in Figure 7.

In view of these issues, a likely scenario is a mix of the different effects discussed above, as indicated in Figure 11e. Our study highlights that the interpretation of the relation between traditional seismological stress drop measurements and the between-event residuals from GMPEs may not be that straightforward and can only be fair if made sure that no data subsets show bias in either $\Delta\tau$ or δB_e. We have shown that there is with no doubt a correlation relationship, which is not really a surprise; however, the generation of the two δB_e families in terms of $\Delta\tau$ dependence proves that it may be problematic integrating different regions, in particular when these regions only show a weak connection in terms of overlapping source-site travel paths. The problem will even be aggravated when mixing $\Delta\tau$ estimates from different studies, obtained using different methodologies and/or reference conditions. *Sonley and Abercrombie* [2006], for instance, discussed the issue of comparing source parameters from different studies focusing on attenuation correction of single spectra. In that case, the generation of different such families in the δB_e-$\Delta\tau$ relationship is practically inevitable.

While we are able to substantially reduce the gap between $\Delta\tau$ and δB_e variabilities by this combined analysis that allows to identify and eliminate inconsistencies between two data sets, the $\Delta\tau$ variability still remains substantially larger than expected from the δB_e variability. Possible physical explanations could lie in effects not accounted for in stress drop calculations, such as an anticorrelation of stress drop and rupture velocity [*Causse and Song*, 2015] or the complexity of the moment rate function combined with attenuation that masks the double corner frequency nature of the source spectra [*Archuleta and Ji*, 2016]. While the former hypothesis cannot be easily checked from a spectral analysis point of view, the source spectra can of course be checked for deviations from the single corner frequency ω^{-2} model. *Uchide and Imanishi* [2016] find from multiple spectral ratio analysis of small earthquakes in Japan that while some events fit the ω^{-2} model well, many others seem to deviate substantially. They interpret this observation as suggestive for a coexistence of crack-like and asperity-like earthquakes in their study region. Such complexities of the rupture process are a likely factor increasing the variability in $\Delta\tau$ estimates from a simple ω^{-2} model fit. However, in view of the common bandwidth limitations, the large degree of variability typically observed in spectral analysis, and other complicating effects such as directivity, it is not trivial to robustly resolve two corner frequencies in view of the often rather subtle deviations from the ω^{-2} fit. This holds particularly true for the source spectral estimates of small earthquakes, where these two-corner frequencies might be expected to be relatively close to each other.

Our results provide insights into the observation of *Cotton et al*. [2013] that the estimated $\Delta\tau$ variability from δB_e is much smaller than from classical M_0-f_C analysis. One aspect is certainly the generation of these families, which are likely to be present in many large-scale data sets combing $\Delta\tau$ and δB_e measurements. The between-event variability of ground motions should therefore be interpreted with caution in terms of $\Delta\tau$ variability, in particular for mixed data sets combing data from different regions. This study shows that a key aspect toward improving our understanding on how much of the observed source parameter variability is likely to be true source physics variability lies in the common detailed analysis of $\Delta\tau$ and δB_e data. It opens the possibility to identify peculiarities in both distributions that may otherwise remain unnoticed and provides consistency checks and hints as to which parts of a given data set and model should be further scrutinized.

Acknowledgments

We wish to thank the National Institute for Earth Science and Disaster Resilience (NIED) for making the K-NET and KiK-net data available. All data used in this study can be freely downloaded following registration on the website http://www.kyoshin.bosai.go.jp/. A. Oth would also like to thank the Earthquake Research Institute of the University of Tokyo for hosting him as a visiting researcher during the time when most of this work has been carried out. We are grateful to the Editor and two anonymous reviewers of this paper for comments that helped to improve the quality of the manuscript. Figure 1 was drawn using the Generic Mapping Toolbox (GMT) [*Wessel and Smith*, 1998].

References

Abercrombie, R. E. (2013), Comparison of direct and coda wave stress drop measurements for the Wells, Nevada, earthquake sequence, *J. Geophys. Res. Solid Earth*, *118*, 1458–1470, doi:10.1029/2012JB009638.

Abercrombie, R. E. (2015), Investigating uncertainties in empirical Green's function analysis of earthquake source parameters, *J. Geophys. Res. Solid Earth*, *120*, 4263–4277, doi:10.1002/2015JB011984.

Abrahamson, N. A., and R. R. Youngs (1992), A stable algorithm for regression analyses using the random effects model, *Bull. Seismol. Soc. Am.*, *82*, 505–510.

Aki, K. (1967), Scaling law of seismic spectrum, *J. Geophys. Res.*, *72*, 1217–1231, doi:10.1029/JZ072i004p01217.

Al Atik, L., N. Abrahamson, J. J. Bommer, F. Scherbaum, F. Cotton, and N. Kuehn (2010), The variability of ground-motion prediction models and its components, *Seismol. Res. Lett.*, *81*, 794–801, doi:10.1785/gssrl.81.5.794.

Anderson, J. G., and J. N. Brune (1999), Probabilistic seismic hazard assessment without the ergodic assumption, *Seismol. Res. Lett.*, *70*, 19–28.

Anderson, J. G. (1986), Implication of attenuation for studies of the earthquake source, in *Earthquake Source Mechanics*, vol. 37, edited by S. Das, J. Boatwright, and C. H. Scholz, pp. 311–318, AGU, Washington, D. C.

Anderson, J. G., and S. E. Hough (1984), A model for the shape of the Fourier amplitude spectrum of acceleration at high frequencies, *Bull. Seismol. Soc. Am.*, *74*, 1969–1993.

Aoi, S., B. Enescu, W. Suzuki, Y. Asano, K. Obara, T. Kunugi, and K. Shiomi (2010), Stress transfer in the Tokai subduction zone from the 2009 Suruga Bay earthquake in Japan, *Nat. Geosci.*, *3*, 496–500, doi:10.1038/NGEO885.

Aoi, S., T. Kunugi, H. Nakamura, and H. Fujiwara (2011), Deployment of new strong motion seismographs of K-NET and KiK-net, in *Earthquake Data in Engineering Seismology*, edited by S. Akkar, P. Gülkan, and T. Van Eck, pp. 167–186, Springer, Heidelberg.

Archuleta, R. J., and C. Ji (2016), Moment rate scaling for earthquakes $3.3 \le M \le 5.3$ with implications for stress drop, *Geophys. Res. Lett.*, *43*, 12,004–12,011, doi:10.1002/2016GL071433.

Asano, K., and T. Iwata (2006), Source process and near-source ground motions of the 2005 west off Fukuoka Prefecture earthquake, *Earth Planets Space*, *58*, 93–98, doi:10.1186/BF03351920.

Asano, K., and T. Iwata (2009), Source rupture process of the 2004 Chuetsu, mid-Niigata Prefecture, Japan, earthquake inferred from waveform inversion with dense strong-motion data, *Bull. Seismol. Soc. Am.*, *99*, 123–140, doi:10.1785/0120080257.

Asano, K., and T. Iwata (2011), Source-rupture process of the 2007 Noto Hanto, Japan, earthquake estimated by the joint inversion of strong motion and GPS data, *Bull. Seismol. Soc. Am.*, *101*, 2467–2480, doi:10.1785/0120100254.

Asano, K., and T. Iwata (2016), Source rupture processes of the foreshock and mainshock in the 2016 Kumamoto earthquake sequence estimated from the kinematic waveform inversion of strong motion data, *Earth Planets Space*, *68*, 147, doi:10.1186/s40623-016-0519-9.

Atkinson, G. M. (2006), Single-station sigma, *Bull. Seismol. Soc. Am.*, *96*, 446–455, doi:10.1785/0120050137.

Baltay, A. S., T. C. Hanks, and G. C. Beroza (2013), Stable stress-drop measurements and their variability: Implications for ground-motion prediction, *Bull. Seismol. Soc. Am.*, *103*, 211–222, doi:10.1785/0120120161.

Bates, D., M. Mächler, B. M. Bolker, and S. C. Walker (2014), Fitting linear mixed-effects models using lme4. arXiv preprint, arXiv:1406.5823.

Bindi, D., S. Parolai, A. Oth, K. Abdrakhmatov, A. Muraliev, and J. Zschau (2011), Intensity prediction equations for Central Asia, *Geophys. J. Int.*, *187*, 327–337, doi:10.1111/j.1365-246X.2011.05142.x.
Boatwright, J. (2007), The persistence of directivity in small earthquakes, *Bull. Seismol. Soc. Am.*, *97*, 1850–1861, doi:10.1785/0120050228.
Bommer, J. J., and N. A. Abrahamson (2006), Why do modern probabilistic seismic-hazard analyses often lead to increased hazard estimates?, *Bull. Seismol. Soc. Am.*, *96*, 1967–1977, doi:10.1785/0120060043.
Boore, D. M. (2003), Simulation of ground motion using the stochastic method, *Pure Appl. Geophys.*, *160*, 635–676.
Boore, D. M., E. M. Thompson, and H. Cadet (2011), Regional correlations of VS30 and velocities averaged over depths less than and greater than 30 meters, *Bull. Seismol. Soc. Am.*, *101*, 3046–3059, doi:10.1785/0120110071.
Boore, D. M., J. P. Stewart, E. Seyhan, and G. M. Atkinson (2014), NGA-West2 equations for predicting PGA, PGV, and 5% damped PSA for shallow crustal earthquakes, *Earthquake Spectra*, *30*, 1057–1085, doi:10.1193/070113EQS184M.
Bozorgnia, Y., et al. (2014), NGA-West2 research project, *Earthquake Spectra*, *30*, 973–987, doi:10.1193/072113EQS209M.
Brune, J. N. (1970), Tectonic stress and the spectra of seismic shear waves from earthquakes, *J. Geophys. Res.*, *75*, 4997–5009.
Brune, J. N. (1971), Correction, *J. Geophys. Res.*, *76*, 5002.
Building Seismic Safety Council (2003), The 2003 NEHRP recommended provisions for new buildings and other structures. Part 1: Provisions (FEMA 450).
Castro, R. R., J. G. Anderson, and S. K. Singh (1990), Site response, attenuation and source spectra of *S* waves along the Guerrero, Mexico, subduction zone, *Bull. Seismol. Soc. Am.*, *80*, 1481–1503.
Causse, M., and S. G. Song (2015), Are stress drop and rupture velocity of earthquakes independent? Insight from observed ground motion variability, *Geophys. Res. Lett.*, *42*, 7383–7389, doi:10.1002/2015GL064793.
Chen, L., and E. Faccioli (2013), Single-station standard deviation analysis of 2010–2012 strong-motion data from the Canterbury region, New Zealand, *Bull. Earthquake Eng.*, *11*, 1617–1632, doi:10.1007/s10518-013-9454-3.
Chen, Y.-H., and C.-C. P. Tsai (2002), A new method for estimation of the attenuation relationship with variance components, *Bull. Seismol. Soc. Am.*, *92*, 1984–1991, doi:10.1785/0120010205.
Cirella, A., A. Piatanesi, E. Tinti, and M. Cocco (2008), Rupture process of the 2007 Niigata-ken Chuetsu-oki earthquake by non-linear joint inversion of strong motion and GPS data, *Geophys. Res. Lett.*, *35*, L16306, doi:10.1029/2008GL034756.
Cotton, F., R. Archuleta, and M. Causse (2013), What is sigma of the stress drop?, *Seismol. Res. Lett.*, *84*, 42–48, doi:10.1785/0220120087.
Cultrera, G., G. Ameri, A. Sarao, A. Cirella, and A. Emolo (2013), Ground-motion simulations within ShakeMap methodology: Application to the 2008 Iwate-Miyagi Nairiku (Japan) and 1980 Irpinia (Italy) earthquakes, *Geophys. J. Int.*, *193*, 220–237, doi:10.1093/gji/ggs074.
Douglas, J. (2003), Earthquake ground motion estimation using strong-motion records: A review of equations for the estimation of peak ground acceleration and response spectral ordinates, *Earth Sci. Rev.*, *61*, 43–104.
Drouet, S., S. Chevrot, F. Cotton, and A. Souriau (2008), Simultaneous inversion of source spectra, attenuation parameters, and site responses: Application to the data of the French accelerometric network, *Bull. Seismol. Soc. Am.*, *98*, 198–219, doi:10.1785/0120060215.
Hanks, T. C. (1982), f_{max}, *Bull. Seismol. Soc. Am.*, *72*, 1867–1879.
Hanks, T. C., and R. K. McGuire (1981), The character of high-frequency strong ground motion, *Bull. Seismol. Soc. Am.*, *71*, 2071–2095.
Hata, Y., A. Murata, A. Nozu, and M. Miyajima (2012), Ground motion evaluation at Yokokura village for the 2011 Nagano-Niigata border earthquake based on the site-effect substitution method, *J. Japan Assoc. Earthq. Eng.*, *12*(2), 60–77, doi:10.5610/jaee.12.2_60.
Hayes, G. (2011), Updated result of the Mar 9, 2011 M_w 7.3 earthquake offshore Honshu, Japan (Tohoku EQ foreshock). [Available at http://earthquake.usgs.gov/earthquakes/eqinthenews/2011/usb0001r57/finite_fault.php, last accessed September 2013.]
Hikima, K., and K. Koketsu (2005), Rupture processes of the 2004 Chuetsu (mid-Niigata prefecture) earthquake, Japan: A series of events in a complex fault system, *Geophys. Res. Lett.*, *32*, L18303, doi:10.1029/2005GL023588.
Horikawa, H. (2001), Earthquake doublet in Kagoshima, Japan: Rupture of asperities in a stress shadow, *Bull. Seismol. Soc. Am.*, *91*, 112–127, doi:10.1785/0119990131.
Iwata, T., H. Sekiguchi, Y. Matsumoto, H. Miyake, and K. Irikura (2000), Source process of the 2000 western Tottori Prefecture earthquake and near-source strong ground motion, paper presented at 2000 Fall Meeting Seismol. Soc. of Japan.
Joyner, W. B., and D. M. Boore (1981), Peak horizontal acceleration and velocity from strong-motion records including records from the 1979 Imperial Valley, California, earthquake, *Bull. Seismol. Soc. Am.*, *71*, 2011–2011.
Kane, D. L., P. M. Shearer, B. P. Goertz-Allmann, and F. L. Vernon (2013), Rupture directivity of small earthquakes at Parkfield, *J. Geophys. Res. Solid Earth*, *118*, 212–221, doi:10.1029/2012JB009675.
Kobayashi, H., K. Koketsu, and H. Miyake (2016), Rupture processes of the 2016 Kumamoto earthquakes derived from joint inversion of strong-motion, teleseismic, and geodetic data. JpGU Meeting 2016, MIS34-MIP65.
Kodera, Y., J. Saitou, N. Hayashimoto, S. Adachi, M. Morimoto, Y. Nishimae, and M. Hoshiba (2016), Earthquake early warning for the 2016 Kumamoto earthquake: Performance evaluation of the current system and the next-generation methods of the Japan Meteorological Agency, *Earth Planets Space*, *68*, 202, doi:10.1186/s40623-016-0567-1.
Kotha, S. R., D. Bindi, and F. Cotton (2016), Partially non-ergodic region specific GMPE for Europe and Middle-East, *Bull. Earthquake Eng.*, *14*, 1245–1263, doi:10.1007/s10518-016-9875-x.
Ktenidou, O.-J., F. Cotton, N. A. Abrahamson, and J. G. Anderson (2014), Taxonomy of κ: A review of definitions and estimation approaches targeted to applications, *Seismol. Res. Lett.*, *85*(1), 135–146, doi:10.1785/0220130027.
Kubo, H., W. Suzuki, S. Aoi, and H. Sekiguchi (2016), Source rupture processes of the 2016 Kumamoto, Japan, earthquakes estimated from strong-motion waveforms, *Earth Planets Space*, *68*, 161, doi:10.1186/s40623-016-0536-8.
Kurzon, I., F. L. Vernon, Y. Ben-Zion, and G. Atkinson (2014), Ground motion prediction equations in the San Jacinto fault zone: Significant effects of rupture directivity and fault zone amplification, *Pure Appl. Geophys.*, *171*, 3045–3081, doi:10.1007/s00024-014-0855-2.
Luzi, L., D. Bindi, R. Puglia, F. Pacor, and A. Oth (2014), Single-station sigma for Italian strong-motion stations, *Bull. Seismol. Soc. Am.*, *104*, 467–483, doi:10.1785/0120130089.
Mai, P. M., and K. K. S. Thingbaijam (2014), SRCMOD: An online database of finite-fault rupture models, *Seismol. Res. Lett.*, *85*, 1348–1357, doi:10.1785/0220140077.
Mayeda, K., L. Malagnini, and W. Walter (2007), A new spectral ratio method using narrowband coda envelopes: Evidence for non-self-similarity in the Hector Mine sequence, *Geophys. Res. Lett.*, *34*, L11303, doi:10.1029/2007GL030041.
McGuire, R. K., and T. C. Hanks (1980), RMS accelerations and spectral amplitudes of strong ground motion during the San Fernando, California earthquake, *Bull. Seismol. Soc. Am.*, *70*, 1907–1919.
Miuara, S., Y. Suwa, T. Sato, K. Tachibana, and A. Hasegawa (2004), Slip distribution of the 2003 northern Miyagi earthquake (*M*6.4) deduced from geodetic inversion, *Earth Planets Space*, *56*, 95–101.

Musson, R. M. W., and I. Cecić (2012), Intensity and intensity scales, in *New Manual of Seismological Observatory Practice (NMSOP-2)*, edited by P. Bormann, chap. 12, pp. 1–41, GFZ German Res. Cent. for Geosci., Potsdam, doi:10.2312/GFZ.NMSOP-2_CH12.

Okada, Y., K. Kasahara, S. Hori, K. Obara, S. Sekiguchi, H. Fujiwara, and A. Yamamoto (2004), Recent progress of seismic observation networks in Japan-Hi-net, F-net, K-NET and KiK-net, *Earth Planets Space*, *56*, 15–28.

Oth, A. (2013), On the characteristics of earthquake stress release variations in Japan, *Earth Planet. Sci. Lett.*, *377-378*, 132–141, doi:10.1016/j.epsl.2013.06.037.

Oth, A., S. Parolai, and D. Bindi (2011a), Spectral analysis of K-NET and KiK-net data in Japan, part I: Database compilation and peculiarities, *Bull. Seismol. Soc. Am.*, *101*, 652–666, doi:10.1785/0120100134.

Oth, A., D. Bindi, S. Parolai, and D. Di Giacomo (2011b), Spectral analysis of K-NET and KiK-net data in Japan, part II: On attenuation characteristics, source spectra, and site response of borehole and surface stations, *Bull. Seismol. Soc. Am.*, *101*, 667–687, doi:10.1785/0120100135.

Rodriguez-Marek, A., G. A. Montalva, F. Cotton, and F. Bonilla (2011), Analysis of single-station standard deviation using the KiK-net data, *Bull. Seismol. Soc. Am.*, *101*, 1242–1258, doi:10.1785/0120100252.

Sekiguchi, H., and T. Iwata (2001), Rupture process of the 2001 Geiyo earthquake obtained from strong motion data [Ver. 1]. [Available at http://sms.dpri.kyoto-u.ac.jp/iwata/zisin/geiyo-e.html, last accessed November 2016.]

Shabestari, K. T., and F. Yamazaki (2001), A proposal of instrumental seismic intensity scale compatible with MMI evaluated from three-component acceleration records, *Earthquake Spectra*, *17*, 711–723, doi:10.1193/1.1425814.

Shearer, P. M., G. A. Prieto, and E. Hauksson (2006), Comprehensive analysis of earthquake source spectra in Southern California, *J. Geophys. Res.*, *111*, B06303, doi:10.1029/2005JB003979.

Sokolov, V., and T. Furumura (2008), Comparative analysis of two methods for instrumental intensity estimations using the database accumulated during recent large earthquakes in Japan, *Earthquake Spectra*, *24*, 513–532, doi:10.1193/1.2923918.

Sonley, E., and R. E. Abercrombie (2006), Effects of methods of attenuation correction on source parameter determination, in *Earthquakes: Radiated Energy and the Physics of Faulting*, vol. 170, edited by R. E. Abercrombie et al., pp. 91–97, AGU, Washington, D. C.

Stafford, P. J. (2014), Crossed and nested mixed-effects approaches for enhanced model development and removal of the ergodic assumption in empirical ground-motion models, *Bull. Seismol. Soc. Am.*, *104*, 702–719, doi:10.1785/0120130145.

Uchide, T., and K. Imanishi (2016), Small earthquakes deviate from the omega-square model as revealed by multiple spectral ratio analysis, *Bull. Seismol. Soc. Am.*, *106*, 1357–1363, doi:10.1785/0120150322.

Wald, D. J., V. Quitoriano, T. H. Heaton, H. Kanamori, C. W. Scrivner, and C. B. Worden (1999), TriNet "ShakeMaps": Rapid generation of peak ground motion and intensity maps for earthquakes in Southern California, *Earthquake Spectra*, *15*, 537–555, doi:10.1193/1.1586057.

Wessel, P., and W. H. F. Smith (1998), New, improved version of the generic mapping tools released, *Eos. Trans. AGU*, *79*, 579.